Identifying Geographical Patterns of Transient Deformation in the Geological Sea Level Record

Simon, K. M.; Riva, R. E.M.; Broerse, T.

DOI
10.1029/2021JB023693

Publication date
2022

Document Version
Final published version

Published in
Journal of Geophysical Research: Solid Earth

Citation (APA)
Simon, K. M., Riva, R. E. M., & Broerse, T. (2022). Identifying Geographical Patterns of Transient Deformation in the Geological Sea Level Record. *Journal of Geophysical Research: Solid Earth*, *127*(7), Article e2021JB023693. https://doi.org/10.1029/2021JB023693

JGR Solid Earth

RESEARCH ARTICLE
10.1029/2021JB023693

Identifying Geographical Patterns of Transient Deformation in the Geological Sea Level Record

K. M. Simon[1,2], **R. E. M. Riva**[1], **and T. Broerse**[3]

[1]Department of Geoscience and Remote Sensing, Delft University of Technology, Delft, The Netherlands, [2]NIOZ Royal Netherlands Institute for Sea Research, Yerseke, The Netherlands, [3]Department of Geosciences, Utrecht University, Utrecht, The Netherlands

Key Points:

- We compare glacial isostatic adjustment (GIA) model predictions with Maxwell and Burgers rheologies to relative sea level data
- Models with Burgers rheology can yield better fits to sea level data, particularly around the west coast of North America
- Transient deformation should be another process of interest in GIA models, especially in the near-field

Supporting Information:

Supporting Information may be found in the online version of this article.

Correspondence to:

K. M. Simon,
k.m.simon@tudelft.nl

Citation:

Simon, K. M., Riva, R. E. M., & Broerse, T. (2022). Identifying geographical patterns of transient deformation in the geological sea level record. *Journal of Geophysical Research: Solid Earth*, *127*, e2021JB023693. https://doi.org/10.1029/2021JB023693

Received 23 NOV 2021
Accepted 21 JUN 2022

Author Contributions:

Conceptualization: K. M. Simon, R. E. M. Riva
Formal analysis: K. M. Simon, R. E. M. Riva, T. Broerse
Methodology: K. M. Simon
Software: T. Broerse
Writing – original draft: K. M. Simon
Writing – review & editing: K. M. Simon, R. E. M. Riva, T. Broerse

Abstract In this study, we examine the effect of transient mantle creep on the prediction of glacial isostatic adjustment (GIA) signals. Specifically, we compare predictions of relative sea level (RSL) change from GIA from a set of Earth models in which transient creep parameters are varied in a simple Burgers model to a reference case with a Maxwell viscoelastic rheology. The model predictions are evaluated in two ways: first, relative to each other to quantify the effect of parameter variation, and second, for their ability to reproduce well-constrained sea level records from selected locations. Both the resolution and geographic location of the RSL observations determine whether the data can distinguish between model cases. Model predictions are most sensitive to the inclusion of transient mantle deformation in regions that are near-field and peripheral relative to former ice sheets. This sensitivity appears particularly true along the North American west coast in the region of the former Cordilleran Ice Sheet, which experienced rapid sea-level fall following deglaciation between 14 and 12 kyr BP. Relative to the Maxwell case, Burgers models better reproduce this rapid phase of regional postglacial sea-level fall. As well, computed goodness-of-fit values in this region show a clear preference for models where transient deformation is present in the whole or lower mantle, and for models where the rigidity of the Kelvin element is weakened relative to the rigidity of the Maxwell element. In contrast, model predictions of relative sea-level change in the far-field show weak sensitivity to the inclusion of transient deformation.

Plain Language Summary In this study, we compare glacial isostatic adjustment (GIA) model predictions using two different Earth model types: Maxwell and Burgers models. Maxwell models are commonly used in GIA studies and employ a time-invariant (steady-state) form of mantle creep. Burgers models, on the other hand, allow for time-varying mantle deformation and include both steady-state and transient components of mantle creep. To evaluate the models, the predictions from both model types are compared to high quality records of relative sea level (RSL) change over the last several thousand years. Burgers models that include transient (time-varying) mantle deformation often fit the RSL data as well as, or better, than the Maxwell models. In particular, the fit between predictions and data is improved in regions that were beneath or near former ice sheets, for example, along the west coast of North America. This result suggests that transient mantle deformation should be considered an additional process of interest in GIA models, especially in regions near the former ice sheets.

1. Introduction

Glacial isostatic adjustment (GIA) modeling requires the application of a space-time varying description of ice sheet evolution to a numerical description of Earth's structure and its associated deformation mechanism (e.g., Lambeck et al., 1998; Peltier, 2004; Peltier et al., 2015; Tushingham & Peltier, 1991). In GIA studies, it is often assumed that Earth deformation is well-described by the deformation of a one-dimensional, radially stratified Maxwell viscoelastic body (e.g., Peltier, 1974), in part because this assumption provides a straightforward and often highly effective description of observed postglacial sea level changes (Peltier et al., 1980). Increasingly though, 3D Earth models are used to account for heterogeneous lithosphere structure (e.g., Spada et al., 2006). As well, more complex rheological models with transient creep (Caron et al., 2017) or steady-state nonlinear mantle viscosities are sometimes implemented (D'Agostino et al., 1997; van der Wal et al., 2010; Wu, 1993).

Whereas the inclusion of steady-state nonlinear rheologies in 3D models considers the stress-dependence in GIA problems (e.g., Wu, 1993), the inclusion of a transient rheology considers the non-steady-state viscosity

after load changes. Laboratory experiments on deformation of mantle rocks at high temperatures provide direct observations of an initial phase of reduced strength, and therefore of viscosity, upon initialization of loading stress (Chopra, 1997; Hansen et al., 2021; Hanson & Spetzler, 1994).

From a microphysical viewpoint, different mechanisms have been proposed to explain transient mantle creep, associated with temporally reduced viscosity and recoverable deformation. From oscillatory laboratory experiments and seismic attenuation observations, grain boundary sliding (GBS) has been proposed to play a major role in transient creep (Faul & Jackson, 2015). At grain boundaries, stress changes lead to elastic stress concentrations that may drive diffusion involving GBS. For small strains, this initially involves elastically accommodated GBS. At a prolonged loading state, transient creep may continue as diffusionally assisted GBS (Morris & Jackson, 2009). Both GBS types result in reverse deformation when the load is removed and are thus, at least partially, recoverable types of creep. A different microphysical phenomenon that results in transient deformation at laboratory conditions is dislocation creep. Dislocation creep may lead to transients by interactions between different grains, or by non-steady state dislocation interactions inside grains. In the first case, interactions between grains deforming on either hard or soft slip systems (Karato, 1998, 2021) could lead to a temporal change in material strength during deformation. Alternatively, interactions between dislocations inside grains, and the evolution of dislocation density, lead to gradual hardening of material and thus to transient behavior (Hansen et al., 2021; Wallis et al., 2021). The latter model also predicts recoverable creep, leading to transient deformation when a load is reduced. All of the proposed mechanisms describe a continuous behavior from transient creep to a gradual transition to steady-state deformation rates. Dislocation creep is nonlinearly dependent on stress while transient GBS is linearly dependent on stress. While GBS is grain-size sensitive and is most effective for fine grains, dislocation creep is generally thought to occur at higher stress levels or larger grain sizes compared to GBS (e.g., Ranalli, 1987). However, the degree to which GBS or dislocation creep contribute to transient deformation at mantle conditions is still unresolved (Faul & Jackson, 2015; Hansen et al., 2021; Lau et al., 2020).

Transient behavior has been observed after large earthquakes in both surface displacements as well as gravity changes, with reduced effective viscosity following the coseismic change of stress in the mantle. Therefore, post-seismic deformation studies (Broerse et al., 2015; Freed et al., 2012; Han et al., 2008; Hoechner et al., 2011; Muto et al., 2019; Pollitz, 2005) regularly employ models with a component of transient mantle creep. Furthermore, transient relaxation is also suggested to be of importance for Earth deformation due to recent rapid glacier melting (Adhikari et al., 2021; Ivins et al., 2020). Many modeling efforts have used the simple four-parameter Burgers model to capture transient creep because its linear biviscous nature allows for both transient and steady-state viscous mantle relaxation without the introduction of much more numerical complexity relative to Maxwell viscoelastic deformation (Section 2). Previously, the simple Burgers model (SBM) has also been used to describe experimental olivine deformation (Chopra, 1997; Smith & Carpenter, 1987). The need to explain transient behavior over a wide range of timescales, mostly shorter than that of GIA (i.e., seismic waves and solid earth tides), has recently lead to the introduction of the extended Burgers model (EBM) (Faul & Jackson, 2015; Ivins et al., 2020; Lau et al., 2020).

In the context of long-term GIA, several publications in the 1980s discussed the effect of transient deformation in the mantle on the prediction of long-term GIA observables (Peltier, 1985; Peltier et al., 1980, 1986; Sabadini et al., 1985; Yuen & Peltier, 1982; Yuen et al., 1986), but while Peltier et al. (1980) concluded transient rheology was likely not important for modeling GIA, Yuen et al. (1986) did not rule it out as an important process in the lower mantle. Yuen et al. (1986) for example, noted both that improved constraint on experimentally determined rheological parameters was needed and indicated that in some cases more or better relative sea level (RSL) data may help to distinguish between various model scenarios. After this time, there was comparatively less discussion on the effect of transient rheology on GIA predictions (Caron et al., 2017; Rümpker & Wolf, 1996; Spada et al., 2011); the results of these more recent studies note differences in predictions between Maxwell and other rheological models, but leave open the question of whether Earth models with transient deformation are required to model the GIA process. Moreover, since laboratory-derived models do not provide robust predictions yet on the timescales of transient deformation, it is not clear whether transient creep should be considered.

Since the dedicated attention in the 1980s to the role of transient deformation in GIA, there have been improvements in both the amount and quality of RSL data available (e.g., Khan et al., 2019, more references in Section 3.3) as well as advances in the constraint of ice sheet history (Roy & Peltier, 2018; Whitehouse, 2018). From the microphysical perspective, it is not straightforward to extrapolate laboratory derived flow laws that account for

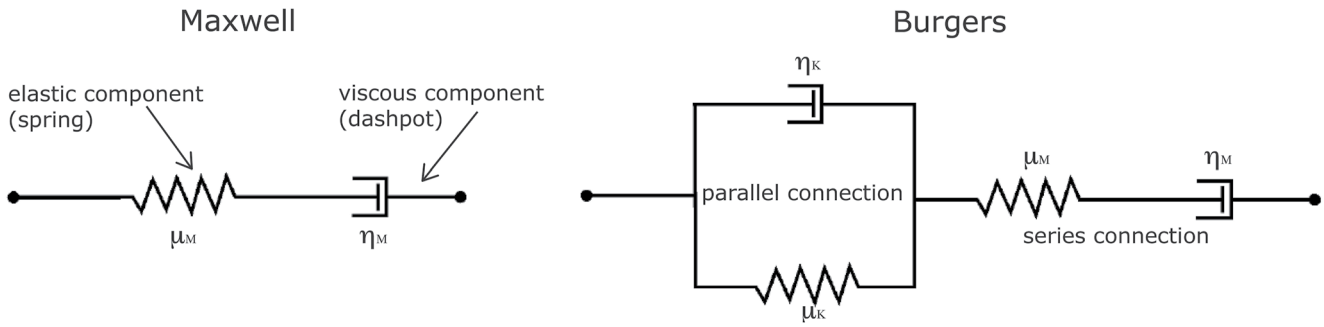

Figure 1. Schematic illustration of Maxwell and four parameter Burgers rheological models. The Maxwell body combines an elastic spring (μ_M) in series with a viscous dashpot (η_M). The Burgers body combines a Maxwell element in series with a Kelvin element in which a spring (μ_K) and dashpot (η_K) are connected in parallel.

transient rheology to mantle conditions. Regarding the transient aspects of dislocation creep, there are still gaps in our understanding of its temporal behavior and the degree of nonlinearity at stress levels applicable for the mantle (Hansen et al., 2021). For the diffusion contribution to transient creep there is considerable uncertainty about how to achieve agreement between laboratory experiments and geodetic constraints on transient deformation (Ivins et al., 2022). However, given the improvements in RSL data and ice histories, we think it is time to revisit the question of how the presence of transient deformation in the mantle may impact GIA predictions, and whether high quality RSL data sets can be expected to distinguish between cases. Ideally, such an examination may also be able to suggest which components of laboratory-measured parameters require improved constraint. Whereas Caron et al. (2017) studied transient deformation in a global inversion context and found that Burgers models do not outperform standard Maxwell models, we suggest that effects of transient rheology will have imprints at specific locations with respect to (former) ice sheets. As changes in ice load are often gradual, we expect that a transient rheology will deviate most from steady-state models where deglaciation is rapid, as in that case the temporal behavior of mantle creep and the temporal evolution of the ice load are best separated. We also expect that in regions with rapid deglaciation, a Burgers model would predict a brief phase of sea level fall that is faster than that predicted by a Maxwell model. Compared to the more complex EBM, for the purpose of studying GIA only, the SBM can provide similar responses (Ivins et al., 2020, see also Section 2). Furthermore, for gradual load changes as can be expected in deglaciation, the response from the EBM resembles mostly a reduction in viscosity without significant temporal complexity (Ivins et al., 2022). This justifies the use of the SBM in our study.

In this study, we compare RSL predictions from a set of Earth models with transient creep in a simple Burgers rheology to a reference case with standard Maxwell rheology. We evaluate the GIA model predictions both relative to each other, as well as their ability to reproduce well-constrained sea level histories from a series of locations. The goal of this research is to address two main questions: (a) Theoretically, as transient rheology variations are incorporated into GIA models, do characteristic differences in RSL change arise with respect to the Maxwell case, and how do the differences depend on geographical region? (b) Practically, when predictions are compared with high quality RSL data, can we identify locations at which transient rheology either plays an important role or at least deserves more attention in GIA models?

The paper is ordered as follows. Section 2 outlines in more detail the physical principles of Maxwell and Burgers body deformation as well as discusses further the choice to employ a SBM. Section 3 describes the Earth and ice model combinations used, as well as the RSL data that are used for comparison. Section 4 provides the modeling results, while Sections 5 and 6 present the discussion and conclusions.

2. Maxwell and Burgers Rheology

Linear rheological models of Earth deformation are conceptualized schematically by combining mechanical elements together in series and/or parallel (e.g., Ranalli, 1987). For example, Maxwell viscoelasticity combines instantaneous elastic deformation with time-dependent steady-state viscous creep by coupling an elastic spring of rigidity μ_M in series with a dashpot of viscosity η_M (Figure 1). In contrast, a Kelvin body consists of a spring (μ_K) connected in parallel to a dashpot (η_K). By coupling a Maxwell body in series with a Kelvin body as in Figure 1,

the four-parameter Burgers body provides the simplest combination of elastic deformation and steady state and transient viscous creep (Burgers, 1935). In this model, the Maxwell part leads to elastic and steady-state viscous deformation, while the Kelvin part provides an initial transient phase of deformation that decays with time. The ratios of the four transient parameters, μ_M/μ_K and η_M/η_K, determine the deformation response of the Burgers model. The ratio μ_M/μ_K is also defined as $\overline{\Delta}$ and is a dimensionless amplitude factor that is a key parameter in the creep function (Ivins et al., 2020). The Kelvin shear modulus and $\overline{\Delta}$ are of practical importance later, as a weaker Kelvin element allows for larger transient creep contributions, and is therefore an important control of model behavior.

To capture geodynamic processes across timescales requires a spectrum of relaxation functions (e.g., Yuen & Peltier, 1982). Such a spectrum can be achieved with the linear EBM, which couples additional Kelvin elements to the simple Burgers case discussed above; as the number of Kelvin elements approaches infinity, the relaxation spectrum becomes continuous and the EBM provides a phenomenological model for mantle deformation at all geodynamic timescales (Ivins et al., 2020; Lau & Holtzman, 2019; Tan et al., 2001; Yuen & Peltier, 1982). EBMs better reproduce solid body tides and may provide a description of mantle deformation that is more consistent with microphysical experiments (Faul & Jackson, 2015). However, under some parameter combinations, model intercomparisons have shown that an EBM can be compatible with a SBM of deformation; specifically, that for higher values of $\overline{\Delta}$ in the SBM, there can exist an analog EBM with similar creep properties (Ivins et al., 2020). As well, for smooth or gradual changes in the applied load, EBMs do not display temporally complex deformation behavior (Ivins et al., 2022). Another possibility is that nonlinear dislocation processes are responsible for transient deformation in GIA. Recent laboratory experiments show that relaxation after stress reductions lead to a transient strain evolution that resembles that of a Burgers rheology (Hansen et al., 2021), even though the long-term viscosity and, possibly, the ratio between transient and steady-state viscosity will be stress-dependent. We therefore find that for our purposes, the simple Burgers body provides an adequate representation of transient mantle rheology since RSL data have a limited time resolution and GIA model predictions are also subject to uncertainty of the applied forcing (i.e., the adopted ice model).

With Burgers body rheology, the transient response to load changes is short-lived, after which the effective viscosity increases and steady-state Maxwell deformation dominates (e.g., Rümpker & Wolf, 1996). Therefore, the timescale of the load changes is important for determining the relative influence of the transient response. In a simple Burgers body, if the time t is sufficiently small, then the effective rigidity and viscosity can be expressed as $\mu_0 = \mu_M$ and $\eta_0 = \frac{\eta_M \eta_K}{\eta_M + \eta_K}$; conversely, if the time is sufficiently large, then $\mu_\infty = \frac{\mu_M \mu_K}{\mu_M + \mu_K}$ and $\eta_\infty = \eta_M$ (Figure S1 in Supporting Information S1), where the M and K subscripts correspond to the Maxwell and Kelvin values, respectively. That is, over shorter timescales, the effective rigidity of the mantle is described by the Maxwell rigidity and for $\eta_M \gg \eta_K$ the effective viscosity approaches the Kelvin viscosity, while over longer timescales, the effective viscosity of the Burgers body converges to the Maxwell viscosity.

For viscoelastic bodies, the stress-strain relations can be written in the Laplace transform domain as (Peltier, 1974)

$$\tilde{\sigma}_{ij} = \tilde{\lambda}(s)\tilde{\epsilon}_{kk}\delta_{ij} + 2\tilde{\mu}(s)\tilde{\epsilon}_{ij}$$

where σ_{ij} is the deviatoric stress, ϵ_{ij} is the deviatoric strain, s is the Laplace transform variable (inverse relaxation time), $\mu(s)$ and $\lambda(s)$ are the s-dependent functions of the equivalent time domain Lamé parameters μ and λ, δ_{ij} is the Kronecker delta, the tilde denotes the Laplace transform domain, and repeated indices imply summation. The rheological properties of the modeled material are contained within the parameters $\tilde{\mu}(s)$ and $\tilde{\lambda}(s)$. For an incompressible medium, $\tilde{\lambda}(s)$ is not defined since $\tilde{\epsilon}_{kk} = 0$. The rheological properties of a four parameter incompressible Burgers body are then described by the rigidity in the Laplace transform domain (Peltier et al., 1986)

$$\tilde{\mu}(s) = \frac{\mu_M s(s + \mu_K/\eta_K)}{s^2 + \left[(\mu_M + \mu_K)/\eta_K + \mu_M/\eta_M\right] s + (\mu_M \mu_K/\eta_M \eta_K)}$$

whereas for the simpler Maxwell case, the rigidity is expressed as

$$\tilde{\mu}(s) = \frac{\mu_M s}{s + \mu_M/\eta_M}.$$

Table 1
Summary of 26 Earth Models Used

Starting Model	Transient Layer(s) in Mantle?	μ_M/μ_K	η_M/η_K
GLOREF	MAX-WM	-	-
GLOREF	BUR-WM	1,10	10,100
GLOREF	BUR-UM	1,10	10,100
GLOREF	BUR-LM	1,10	10,100
SUBDUCTION-REF	MAX-WM	-	-
SUBDUCTION-REF	BUR-WM	1,10	10,100
SUBDUCTION-REF	BUR-UM	1,10	10,100
SUBDUCTION-REF	BUR-LM	1,10	10,100

Note. GLOREF: 96 km thick elastic lithosphere, 5×10^{20} Pa s upper mantle steady-state viscosity, and 1×10^{22} Pa s lower mantle steady-state viscosity. SUBDUCTION-REF: 60 km thick elastic lithosphere, and steady-state viscosities of: 3×10^{18} Pa s uppermost mantle of 140 km thickness, 4×10^{20} Pa s transition zone, 1×10^{22} Pa s lower mantle. MAX = Maxwell, BUR = Burgers, WM = Whole mantle, UM = Upper mantle, and LM = Lower mantle (Note, BUR-UM has MAX-LM and BUR-LM has MAX-UM).

While in general the Kelvin element is expected to be weaker than the Maxwell element (Hetland & Hager, 2006), that is, the contribution of transient deformation is larger than the purely elastic contribution, studies of both post-seismic deformation and GIA have noted the difficulty in reliably constraining parameters relating to Burgers rheology such as the ratios μ_M/μ_K and η_M/η_K (Broerse et al., 2015; Caron et al., 2017). Some ratios implemented in past studies are: $\mu_M/\mu_K = 3.3$, $\eta_M/\eta_K = 10$ (Spada et al., 2011), $\mu_M/\mu_K = 10$, $\eta_M/\eta_K = 10$ (Yuen et al., 1986), $\mu_M/\mu_K = 1$, $\eta_M/\eta_K = 28$ (Pollitz, 2005), and $\mu_M/\mu_K = 3$, $\eta_M/\eta_K = 7.5$ (Broerse et al., 2015).

3. Modeling Setup

3.1. Earth Model Sets

The deformation response of the solid Earth and gravitational potential field is computed using the analytical normal mode method (Broerse et al., 2015; Peltier, 1985; Sabadini et al., 2016; Vermeersen & Sabadini, 1997), while the combined Earth-ice model GIA response is computed with the computer code PGCcalc (James, 1991; Martinec et al., 2018). The Earth models used here are incompressible and consist of five radially symmetric layers. The elastic parameters of the layers are obtained by volume averaging the Preliminary Reference Earth Model (PREM) (Dziewonski & Anderson, 1981).

Two main Earth models form the basis for subsequent parameter variation. The first model we use serves as a global reference model and has a 96-km-thick elastic lithosphere, upper mantle viscosity of 5×10^{20} Pa s, and lower mantle viscosity of 1×10^{22} Pa s. The second Earth model is considered appropriate for the Cascadia subduction zone and has a 60 km thick elastic lithosphere, a 140 km thick and 3×10^{18} Pa s viscosity uppermost mantle, and a 4×10^{20} Pa s transition zone (James, Gowan, Wada, & Wang, 2009); like the first model, the lower mantle is assigned a viscosity of 1×10^{22} Pa s. We select an Earth model consistent with properties of the Cascadia subduction zone because this area represents a regional variation relative to the global case and is also likely an end-member low viscosity model; in Section 4, we compare model predictions to several RSL curves from around the Cascadia subduction zone. Within the two Earth models, we vary three parameters relating to the inclusion of transient deformation: (a) the location of the transient rheology (whole mantle, upper mantle only, and lower mantle only), (b) the rigidity ratio μ_M/μ_K, and (c) the viscosity ratio η_M/η_K (Table 1). Because the ratios are not well-constrained, the models with transient deformation use what can be considered end member values to bracket the plausible range of values. Specifically, we use $\mu_M/\mu_K = 1{,}10$ and $\eta_M/\eta_K = 10{,}100$ for a total of four μ_M/μ_K and η_M/η_K combinations (Table 1). We aim both for models that qualitatively fit the data, as well as end-member Earth model sets that serve to capture the extent to which transient cases may deviate from the standard Maxwell case.

3.2. Choice of Ice Model

The GIA response is calculated by coupling each Earth model to the ice sheet model ICE-7G (https://www.atmosp.physics.utoronto.ca/~peltier/data.php, Roy & Peltier, 2018). In a region west of the Laurentide Ice Sheet

(LIS) that corresponds with the approximate extent of the Cordilleran Ice Sheet (CIS), we introduce a ∼1 kyr forward (later in time) shift in the timing of deglaciation in the ice sheet model. We introduce the timing shift because the volume history of ICE-7G in this region suggests that the model deglaciates earlier than is supported by regional RSL data; this issue is consistent with a noted discrepancy between the margin chronology of the southwestern CIS and regional RSL observations (James et al., 2000).

It is important to realize that like its predecessors, the ICE-7G model was developed to be compatible with a particular description of Earth rheology, and thus the ice sheet and Earth model response are coupled. Relative to the data that constrained the ice sheet model and its Earth model, pairing the ice sheet model with varying Earth models may therefore introduce misfits between model predictions and data that may not be present from pairing the ICE-7G model with its corresponding Earth model. However, in this study, our primary interest is the examination of general behavior introduced by transient creep and not the development of best-fit scenarios; by holding the ice sheet history constant, it is easier to isolate the effects of transient deformation in the mantle.

3.3. Selection of RSL Data

First, we examine the effect of including transient deformation theoretically, by comparing sea-level predictions from transient-included models to the associated Maxwell case, as well as practically, by comparing the sea-level predictions of each model to proxy measurements of RSL at selected locations. As well, we examine the effect of including transient deformation on sea-level change in four geographical categories: (a) near-field, (b) mid-field, (c) far-field, and (d) active subduction zones. The first three categories relate each region relative to its distance from former ice sheets. Subduction zones may be physically located in any of the categories 1–3, but because of their likelihood to be characterized by mantle viscosities well below globally averaged values, they are also considered independently.

For comparison with predictions, we have selected several locations characterized by high quality RSL histories from each of the four geographical categories (Figure 2 and Table S1 in Supporting Information S1). The first four locations (Profile 1) come from the region of the Cascadia subduction zone along the Pacific coastline of North America (Engelhart et al., 2015; Hutchinson et al., 2004; James et al., 2005; James, Gowan, Hutchinson, et al., 2009); these locations are at or near the southwestern margin of the former CIS. Crucially, sites 1–3 of Profile 1 include high quality data that record the very rapid regional uplift that followed retreat of the CIS. The next four locations (Profile 2) run in an approximately north-south profile from at or near the center of the former LIS along the Atlantic coastline of North America to the northern Gulf of Mexico (Engelhart & Horton, 2012; Milliken et al., 2008; Vacchi et al., 2018). Another four sites from Scandinavia, the British Isles, and northern Europe (Profile 3) are located at the center of the former Scandinavian Ice Sheet, the center of the former British-Irish Ice Sheet (BIIS), and the northern coastline of the European mainland (Hijma & Cohen, 2019; Nordman et al., 2015; Shennan et al., 2018). Finally, the far-field sea level history of Barbados is included (Peltier & Fairbanks, 2006) along with an additional far-field sea level history from the Malay-Thai Peninsula (Mann et al., 2019).

Figure 2 indicates the sources of the relative data sets. The data sets at minimum include information about interpreted sea level position, sample age, associated uncertainties of those values, material type, and geographical location. The data points are usually classified as either sea level index points (SLIPs) or marine or terrestrial limiting data. SLIP data are data points that can be interpreted to constrain the vertical position of sea level with discrete lower and upper bounds. Marine (terrestrial) limiting data on the other hand provide only lower (upper) limits on the position of sea level and therefore offer looser constraint on the position of sea level. More about modern reporting protocols for RSL proxy data can be found in Hijma et al. (2015) and Khan et al. (2019).

4. Results

In Section 4.1, we qualitatively compare the RSL predictions both to each other (Section 4.1.1) and to the data (Section 4.1.2) for the GLOREF model set where the whole mantle has a transient rheology. The corresponding cases where transient deformation is included in the upper mantle only and lower mantle only are shown in the Supporting Material (Figures S2–S5 in Supporting Information S1). Section 4.2 quantitatively extends the results of the GLOREF set by presenting goodness-of-fit values relative to the data for the full GLOREF set (WM, UM,

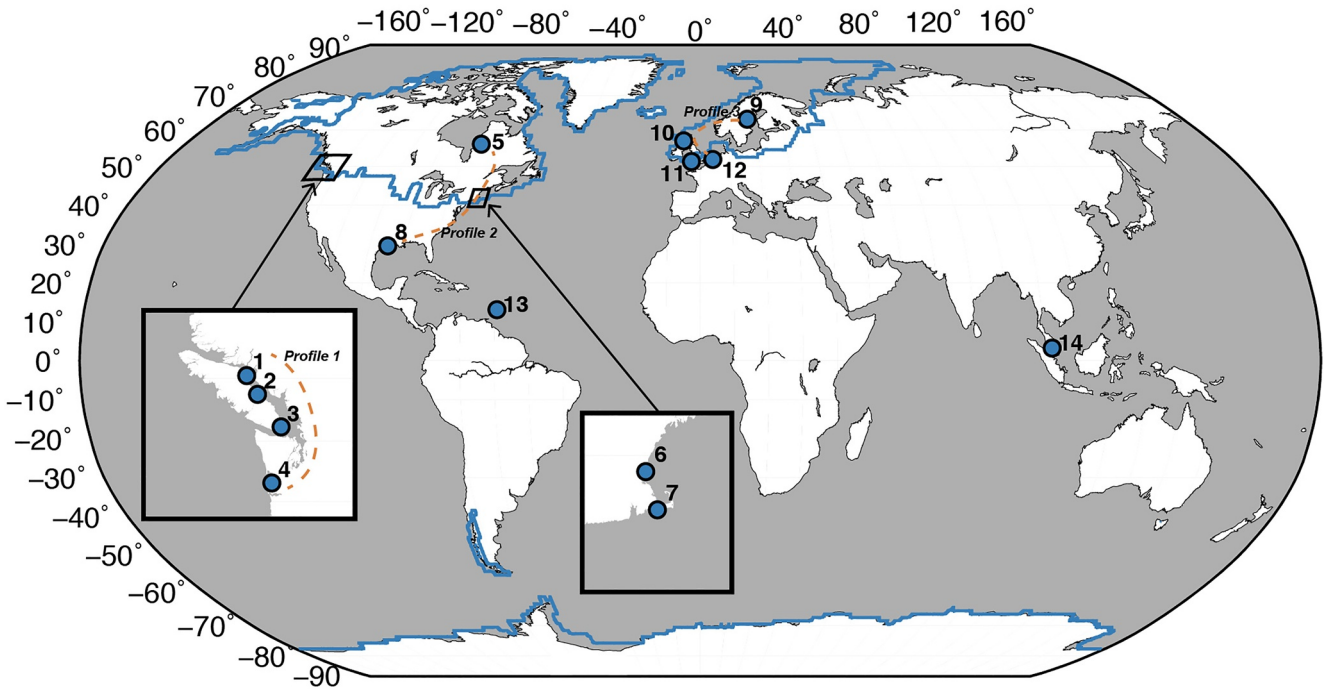

Figure 2. Map of relative sea level histories used in the comparison. Numbers in italics after site names indicate geographical category (*1 = near-field, 2 = mid-field, 3 = far-field, and 4 = subduction zone*). 1 = northern Strait of Georgia (*1*, *4*), 2 = central Strait of Georgia (*1*, *4*), 3 = Victoria (*1*, *4*), 4 = southern Washington coast (*2*, *4*), 5 = Richmond Gulf (*1*), 6 = Boston (*2*), 7 = Barnstable Marsh (*2*), 8 = Northern Gulf of Mexico (*3*), 9 = Ångermanland (*1*), 10 = Arisaig (*1*), 11 = Bristol Channel (*2–3*), 12 = Rotterdam (*2–3*), 13 = Barbados (*3*), and 14 = Malay-Thai Peninsula (*3*). Sources: 1 = James et al. (2005), 2 = Hutchinson et al. (2004), 3 = James, Gowan, Hutchinson, et al. (2009), 4 = Engelhart et al. (2015), 5 = Vacchi et al. (2018), 6–7 = Engelhart and Horton (2012), 8 = Milliken et al. (2008), 9 = Nordman et al. (2015), 10–11 = Shennan et al. (2018), 12 = Hijma and Cohen (2019), 13 = Peltier and Fairbanks (2006), and 14 = Mann et al. (2019). The solid blue lines approximate the ice sheet limits at 26 kyr BP, the dashed orange lines approximate the locations of Profiles 1–3.

and LM). We summarize the results of the subduction zone model set in Section 4.3 and provide figures in the Supporting Material (Figures S6–S13 in Supporting Information S1).

4.1. Predictions of the GLOREF-WM Model Set

4.1.1. Presentation of RSL Predictions and General Trends

Figures 3–5 show relative sea-level predictions for the global reference set for the case where the whole mantle has a transient rheology. Figures 3 and 4 present the Maxwell reference model prediction with the four transient rheology variations (Table 1, MAX-WM and BUR-WM) as well as the associated sea level data for each site, with Figure 3 emphasizing site 2, where the transient variations yield significant differences in response. To provide context relating to the deglaciation history, Figures 4 and 5 also show regional equivalent barystatic sea level values. The regional equivalent sea level histories are calculated for five subregions (Figure S14 in Supporting Information S1): the southwestern CIS (sites 1–3), the central LIS (site 5), the southeast margin of the LIS (sites 6–7), the central Scandinavian Ice Sheet (SIS, site 9), and the BIIS (site 10). The equivalent sea level values are regional and do not estimate the total volume history of any individual ice sheet. Rather, the curves provide information over the timing and speed of regional deglaciation from which we derive approximate time windows that correspond to the period of most ice loss for each region (Figures 4 and 5).

At the full vertical scale of the RSL predictions from all sites, the differences between model predictions are difficult to discern at some sites. The vertical differences between RSL predictions from transient rheology Earth models relative to the reference Maxwell model better highlight the changes yielded by the inclusion of transient deformation (Figure 5). In Figure 5, the RSL data points are likewise differenced in the vertical sense relative to the Maxwell model prediction. Where the model deviation and data deviation relative to the Maxwell case are both large and similar to each other, we find locations at which RSL data should be able to distinguish between steady-state and transient creep models.

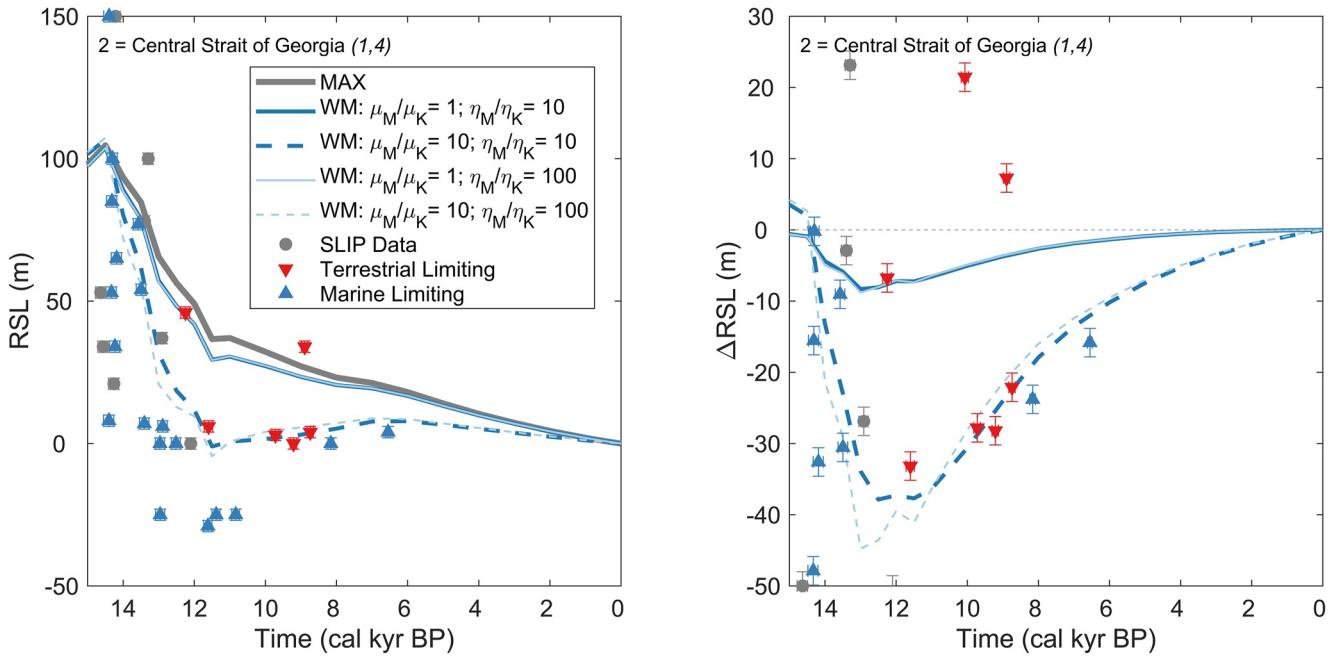

Figure 3. Relative sea level (RSL) predictions (left) and RSL differences relative to the Maxwell case (right) for the GLOREF-WM Earth model set at site 2, Central Strait of Georgia. MAX = Maxwell reference, WM = whole mantle. RSL data are shown as gray circles = sea level index point data, red inverted triangles = terrestrial limiting data, and blue triangles = marine limiting data. Site category follows site name with italicized numbers in brackets (1 = near-field, 2 = mid-field, 3 = far-field, and 4 = subduction zone).

Qualitative comparison of the model predictions to each other reveals some general trends regardless of the quality of available constraining data (Figure 5). Geographically, predicted differences in sea-level are prominent in locations that were either underneath or adjacent to former ice sheets. Farther from the former ice sheets, the variations between models in predicted sea level diminish until there is little observable difference at far-field locations. Where differences between model predictions are present, the models with transient deformation predict a brief phase of faster sea level fall relative to the Maxwell case, after which a recovery to steady-state Maxwell deformation occurs. Weakening of the Kelvin rigidity exerts primary control on the predicted differences in sea level, with the largest differences predicted between models with $\mu_M/\mu_K = 1$ and $\mu_M/\mu_K = 10$. Models with a reduced Kelvin viscosity result in smaller but nonnegligible differences in predicted sea level, with little additional change predicted between models with $\eta_M/\eta_K = 10$ and $\eta_M/\eta_K = 100$. Models with equal Kelvin and Maxwell rigidities ($\mu_M/\mu_K = 1$) show maximum predicted differences in sea level of approximately 10 m (~12%–15% maximum reduction), whereas models with $\mu_M/\mu_K = 10$ predict maximum differences in sea level of more than 40 m (up to ~40%–60% reduction), irrespective of the η_M/η_K ratio.

4.1.2. Comparison of RSL Predictions to Data

Profile 1 runs approximately north-south along and beyond the southwestern margin of the former CIS. Sites 1–3 were all covered by ice during the last glaciation and the sea level proxy data at these sites record rapid postglacial sea level fall (Figures 3 and 4). Site 4 lies close to the southern extent of the CIS and is characterized by observed RSL rise. When transient deformation is included, the largest predicted differences in sea level are observed in the Strait of Georgia and at Victoria (sites 1–3), where model predictions all feature a distinct phase of sea-level fall following deglaciation that is more rapid and brief than that predicted by the Maxwell model. Farther away, at site 4 along the southern Washington coast, similar but muted differences in sea level are predicted. The models with transient rheology better predict RSL change than the Maxwell case for sites 1–3, particularly those with reduced Kelvin rigidity (Figure 5).

Profile 2 spans the region central to the LIS along the US Atlantic coast to the Gulf of Mexico. One region where LIS ice was thickest is around Richmond Gulf (site 5). Here, relative to the Maxwell case, more rapid sea level fall is predicted for the models with a Burgers rheology. In the more load-peripheral locations of Boston and Barnstable Marsh (sites 6–7), the predicted transient-induced changes occur farther back in time where data are

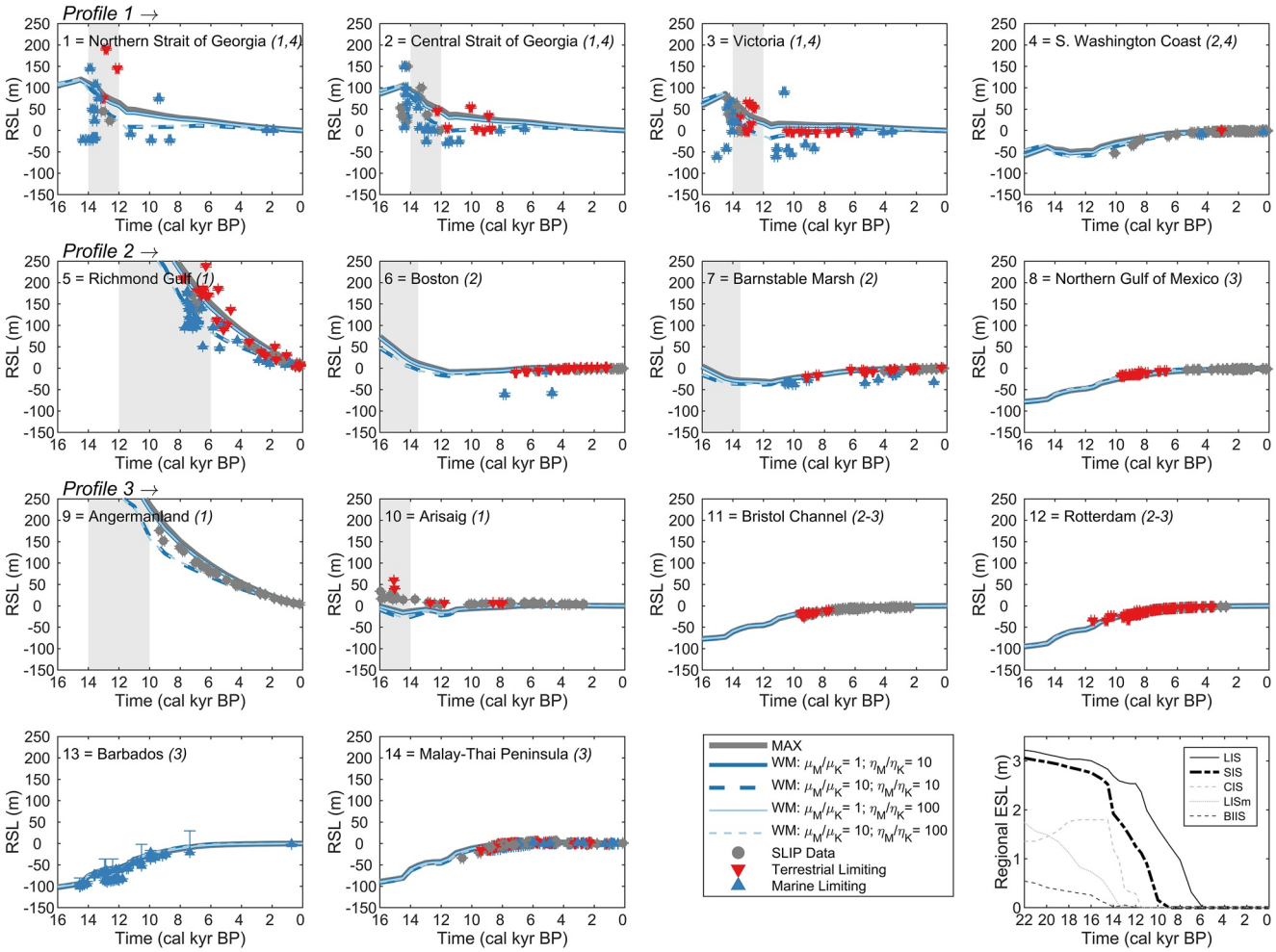

Figure 4. Relative sea level predictions for the GLOREF-WM Earth model set. MAX = Maxwell reference, relative sea level data are shown as gray circles = sea level index point data, red inverted triangles = terrestrial limiting data, and blue triangles = marine limiting data. Site category follows site name with italicized numbers in brackets (1 = near-field, 2 = mid-field, 3 = far-field, and 4 = subduction zone). Gray vertical shading indicates the approximate time window of deglaciation at relevant sites. Regional equivalent sea level values are shown for five regions, as discussed in the text (LIS [m] = Laurentide Ice Sheet [margin], SIS = Scandinavian Ice Sheet, CIS = Cordilleran Ice Sheet, and BIIS = British-Irish Ice Sheet).

sparse. Older sea level indicators would be needed to determine whether the transient rheology predictions are compatible with the observed sea level histories at these locations. At the Gulf of Mexico (site 8) the model predictions differ little, and the data cannot distinguish between model cases.

Profile 3 runs from the center of the former Scandinavia Ice Sheet to regions located within its peripheral forebulge zone. At Ångermanland (site 9), a phase of more rapid sea-level fall is predicted for the transient-included models. At Arisaig (site 10), the models with a reduced Kelvin rigidity provide a moderate change in predicted sea level before 10 kyr BP. However, more importantly at Arisaig, all model predictions underpredict the position of past sea level and fit the data poorly. This result suggests that further revision of the ice sheet history is needed in this region. Neither the predictions at Bristol Channel nor Rotterdam (sites 11–12) differ enough for the RSL data to distinguish between model cases.

The last two specific locations examined are Barbados and the Malay-Thai Peninsula (sites 13–14). Both sites 13 and 14 are located in the far-field relative to past ice sheets, and the inclusion of transient deformation introduces little to no significant difference between the various model predictions at these sites. Importantly, no model violates the fit to the Barbados sea level data set, which is often considered a proxy for global barystatic sea level and used as a volume constraint in global ice sheet models (Peltier & Fairbanks, 2006).

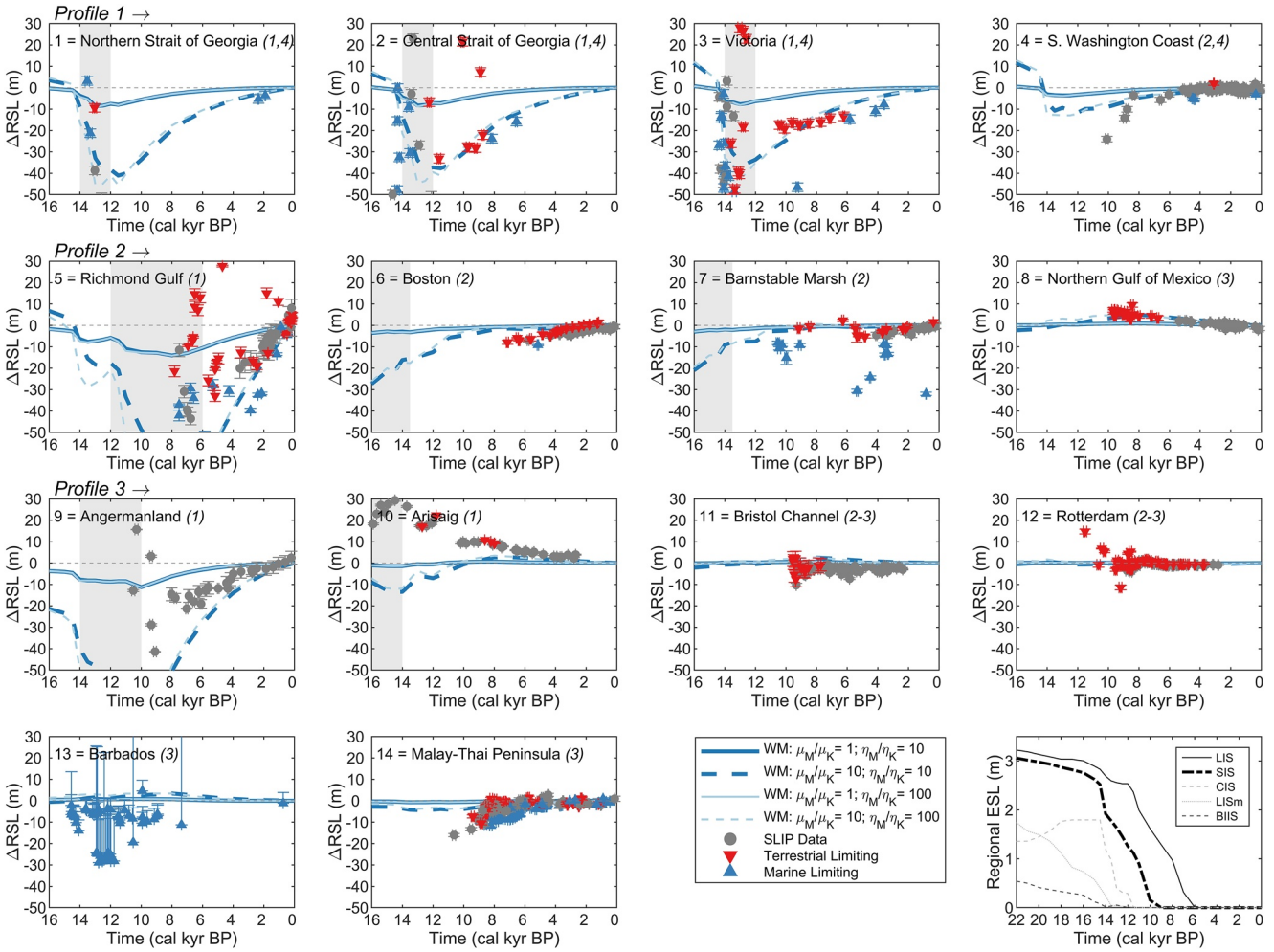

Figure 5. Relative sea level differences relative to the Maxwell reference model for the GLOREF-WM Earth model set. MAX = Maxwell reference, relative sea level data, regional equivalent sea levels, deglaciation time windows, and site categories are shown same as in Figure 4. Note that when differenced relative to the Maxwell case, a few data points plot outside of the given ΔRSL range.

4.2. Goodness-of-Fit Calculations for the GLOREF Set

To extend the qualitative comparison of the RSL predictions to data, we calculate the goodness-of-fit between predictions and data using normalized χ^2 values for the SLIP data, and percent misfit values for the limiting sea level data (Figures 6 and 7). Here, the results for the full global reference model set are provided (i.e., whole mantle, upper mantle, and lower mantle variations are all shown).

For a given RSL curve, the χ^2 values for all SLIP data points follow from

$$\chi^2 = \frac{1}{N}\sum_{i=1}^{N}\left[\left(\frac{y_i - Y_i}{\sigma_{y,i}}\right)^2 + \left(\frac{t_i - T_i}{\sigma_{t,i}}\right)^2\right]$$

where (y_i, t_i) is the RSL position and age of the ith SLIP data point, $(\sigma_{y,i}, \sigma_{t,i})$ are the associated uncertainties of the data point in space and time, (Y_i, T_i) is the model prediction nearest the observed values, and N is the number of SLIP points at each location (e.g., Paulson et al., 2007). The χ^2 values are normalized both relative to the number of SLIP data points as indicated in the above equation, as well as relative to the χ^2 value that provides the worst fit out of the 13-model set. The second normalization allows the results to be compared or ranked in terms of relative model improvement across sites; the normalized χ^2 value of 1 indicates the worst fit of the model set. For each terrestrial (marine) limiting data point, the percent misfit value is assigned cumulatively a value of 100%

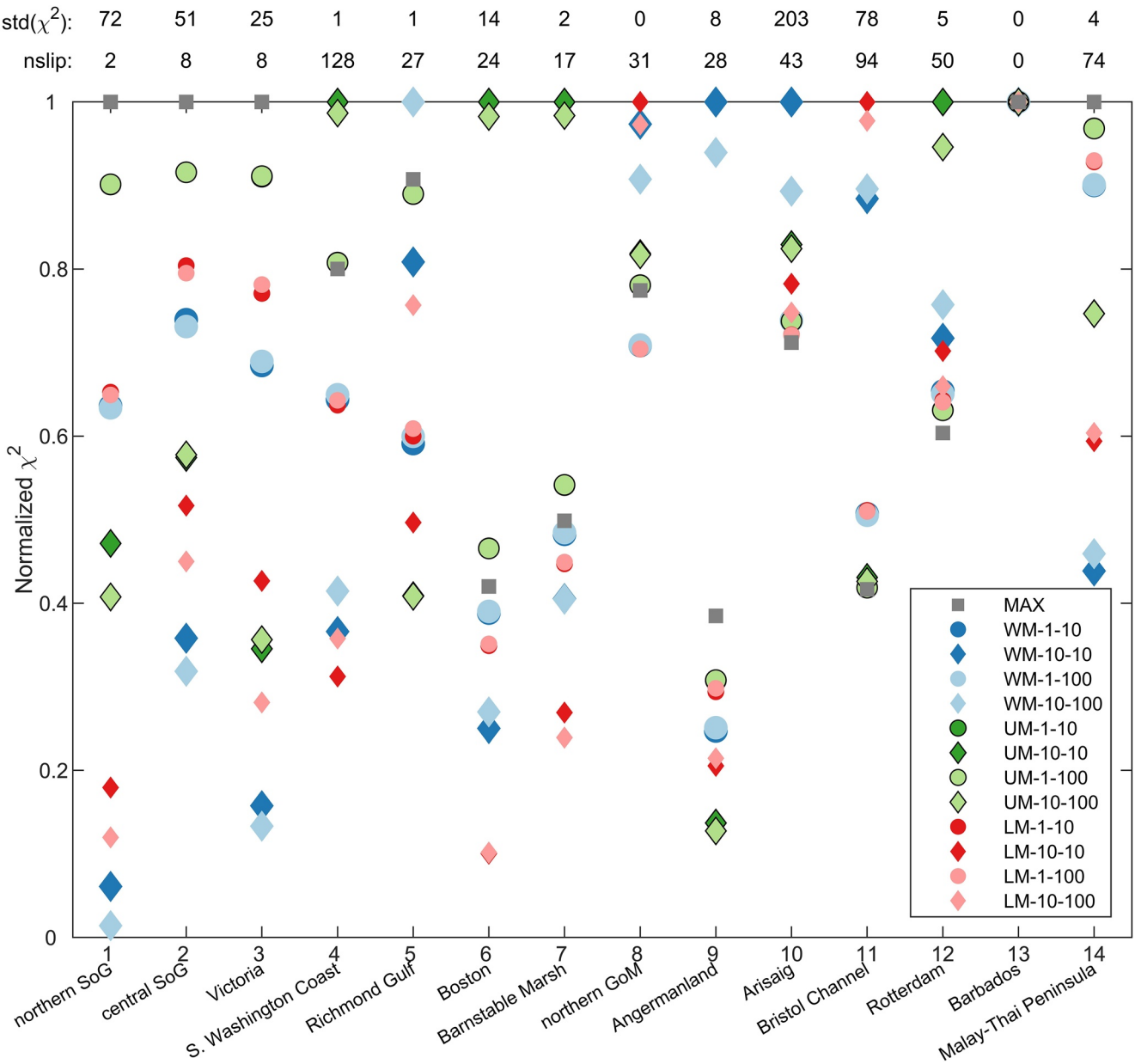

Figure 6. Normalized χ^2 values for the sea level index point (SLIP) data and the GLOREF model set, lower = better. MAX = Maxwell reference, WM = whole mantle, UM = upper mantle, LM = lower mantle, SoG = Strait of Georgia, and GoM = Gulf of Mexico. In the legend, the first number corresponds to the μ_M/μ_K ratio, the second number corresponds to the η_M/η_K ratio. Value for Barbados set to one due to lack of SLIP data points. The total number of SLIP data points and standard deviations of the χ^2 values are given at the top of the plot.

if the model over- (under-) predicts the position of RSL including the uncertainty, and a value of 0% otherwise; the percent misfit value is then normalized by the total number of terrestrial and marine limiting data points for a given RSL curve such that a value of 0% indicates that the model correctly predicts the position of sea level relative to all limiting data points and a value of 100% indicates the opposite. In some cases, there are curves that have either no SLIP data (e.g., Barbados), or little to no limiting data (e.g., Arisaig), in which case only one metric can be calculated reliably. For each location, the standard deviation of the χ^2 values is also given to indicate the significance of the different model rankings (an improved model is more significant if the standard deviations of the χ^2 values are large).

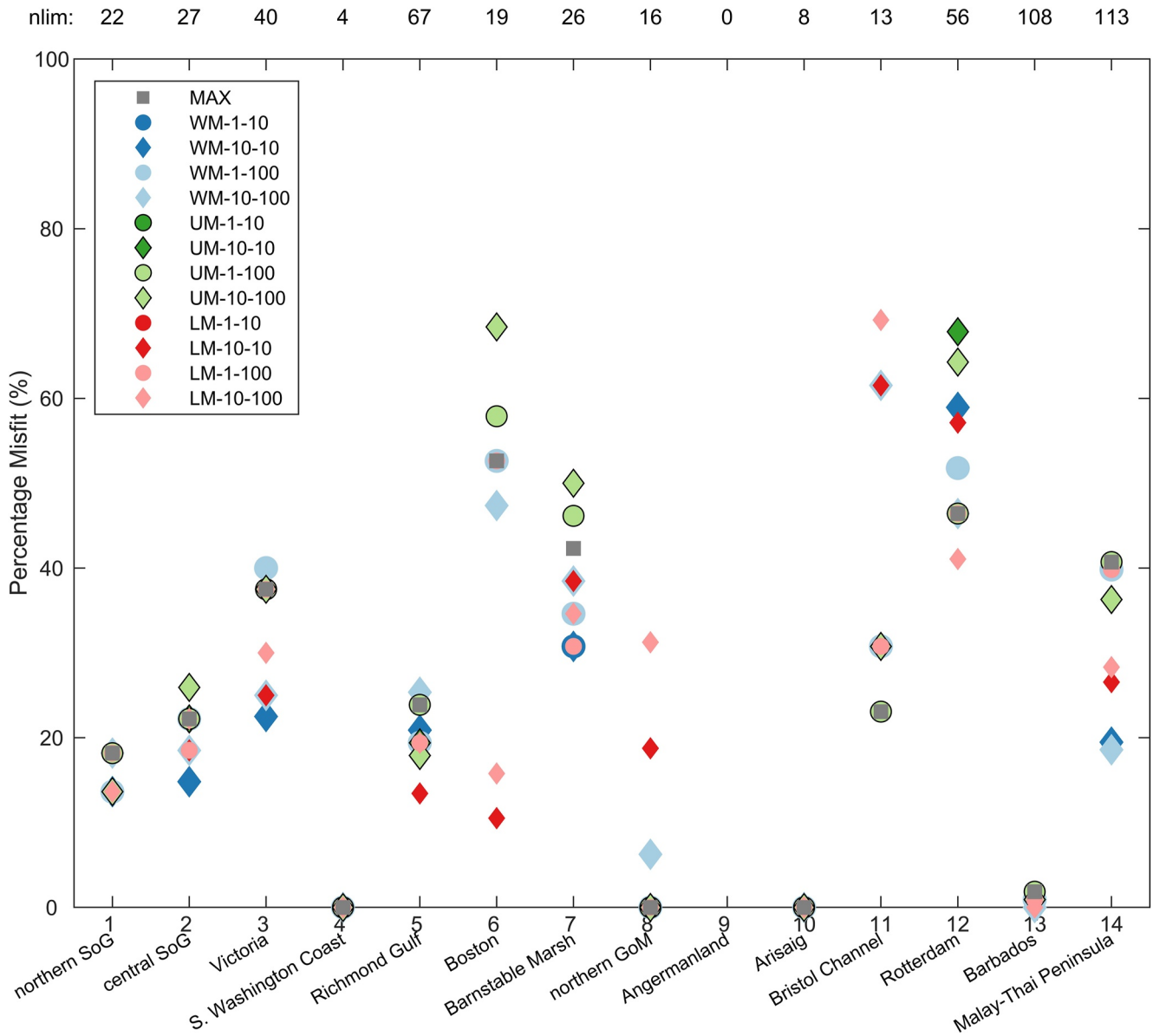

Figure 7. Percent misfit values for the limiting sea level data and the GLOREF model set, lower = better. Abbreviations and model legend are the same as in Figure 6. Misfit values for southern Washington Coast, Ångermanland, and Arisaig are not informative given little to no limiting data. The total number of limiting data points are given at the top of the plot.

The computed χ^2 and percentage misfit values for Profile 1 show a clear preference for models with transient deformation in the whole or lower mantle as well as a weakened rigidity of the Kelvin element. The improved fit is particularly marked for sites 1–3. Smaller improvements in fit for Profile 1 are also achieved for models with transient deformation restricted to the upper mantle and reductions of the viscosity of the Kelvin element. Notably, all transient model variations perform better than the Maxwell case at sites 1–3. The χ^2 values at site four suggest an improvement in fit consistent with sites 1–3, although with a standard deviation of approximately one for these χ^2 values, the improvement is more modest.

Like Profile 1, the χ^2 and percentage misfit values for sites 5–7 of Profile 2 are generally lower for models with transient deformation in the whole or lower mantle and a reduced Kelvin rigidity. However, the largest transient-induced changes at Boston and Barnstable Marsh (sites 6–7) tend to occur at times where data are sparse. At the Gulf of Mexico (site 8), the Maxwell model is one of the best-fitting models, although all model predictions are similar this far from the load center. Moreover, the standard deviations of the computed χ^2 values

for the sites of Profile 2 are relatively small, suggesting that while some transient deformation models perform better overall, the improvement in fit is less significant for Profile 2 than Profile 1.

Along Profile 3, the fit at Ångermanland (site 9) is improved for several of the Burgers models (Figure 6), although notably not for the models with whole mantle transient deformation and reduced Kelvin rigidity; however, as with some other locations, the variation in computed χ^2 values at this site is relatively low. The poor overall fit at Arisaig (site 10) (Figures 4 and 5) is likely driven in part by limitations in the ice sheet model, complicating inferences for a preferred Earth model at this site. The Maxwell model performs well at both Bristol Channel and Rotterdam (sites 11–12), although there is little variation in χ^2 values at Rotterdam. There is a large variation in the χ^2 values at Bristol Channel, although the model predictions do not appear to differ greatly here (Figures 4 and 5); the large variation in the χ^2 values at Bristol Channel may in part reflect the small uncertainties of the sea level data at this site.

Finally, the percentage misfit values suggest that all models fit the data well at Barbados (site 13) (Figure 7). Like at other farther field locations, the model set does not produce very different χ^2 misfit values at the Malay-Thai Peninsula (site 14) (Figure 6), although models with a component of transient deformation fit the limiting data somewhat better at this site (Figure 7).

4.3. The Subduction Zone Model Set

The model predictions and goodness-of-fit values for the subduction zone set are shown in the Supporting Material (Figures S6–S13 in Supporting Information S1). For completeness, model predictions and goodness-of-fit values are shown for all 14 selected sites. However, this set of Earth models is characterized by the low mantle viscosities expected in subduction zones and is therefore only appropriate when applied at the sites in Profile 1.

Along Profile 1, the results for the subduction zone model set are broadly similar to those of the global reference model set. Relative to the global reference Maxwell model, the weaker transition zone and upper mantle of the subduction zone model can yield an improved fit of the Maxwell model predictions to the data (Figures S15 and S16 in Supporting Information S1). The inclusion of transient deformation again produces more rapid sea level fall following deglaciation, and further improves the fit of predictions to data, particularly at sites 1–3. As with the global reference set, the preferred models include transient deformation in the whole or lower mantle and have a reduced Kelvin rigidity, although almost all models with transient deformation provide an improved fit to data relative to the Maxwell case along Profile 1 (Figures S12–S13 in Supporting Information S1).

5. Discussion

The assumption that the Earth's deformation from long-term GIA is well-described by Maxwell viscoelasticity underpins much of GIA research (Lambeck et al., 1998; Peltier, 1974; Peltier et al., 2015). However, both post-seismic deformation studies and rock physics experiments indicate that a Maxwell model misses a transient phase of deformation that is observed after earthquakes as well as in the laboratory (e.g., Faul & Jackson, 2015; Freed et al., 2012; Hanson & Spetzler, 1994; Pollitz, 2005). And while the follow-on generation of Earth models often incorporate increasing complexity, 3D and nonlinear type Earth models can be computationally expensive, and do not always yield improved fits to data relative to simpler 1D Earth models (Marsman et al., 2021). Furthermore, these models have many free and often poorly constrained parameters (e.g., Karato & Wu, 1993) based on extrapolation of empirical relations for steady-state viscous creep, and thereby neglect transient creep. Like Maxwell models, Burgers models are linearly viscous and spherically symmetric. Because these models exploit the power of the analytical normal modes method, SBMs require little to no additional computational expense and the introduction of relatively few additional parameters; however, with their time dependent viscosity, Burgers models also allow for deformation that is sensitive to the timescale of load changes. Compared to nonlinear steady-state rheologies, Burgers models therefore provide an alternative mechanism for a time-varying mantle rheology that is also relatively straightforward to implement.

Our results indicate that relative to Maxwell models, Burgers models predict a transient phase of more rapid sea level fall following deglaciation in regions that were underneath or adjacent to former ice sheets (Figures 3–5). In such regions, over timescales consistent with the long-term GIA process, the model predictions are more sensitive to the ratio between the Maxwell and Kelvin rigidities, and less sensitive to the associated ratio between the

viscosities. We find the best fits to data with rigidity ratios μ_M/μ_K greater than one; this finding further suggests a SBM may be adequate for the long-term GIA process since SBM and EBM models are compatible at higher values of $\overline{\Delta}$ (Ivins et al., 2020). Due to the interference between the timescales of deglaciation and mantle relaxation, it is difficult to constrain absolute values of the Kelvin viscosity. In locations where sea level data exist that constrain postglacial sea level fall, the results generally show that Burgers models can fit the data as well as, or better, than the Maxwell reference case. The global analysis of Caron et al. (2017) concluded that Burgers models do not significantly outperform Maxwell models. In contrast, we find that there are cases in which Burgers models can yield improved fits at a regional scale. Such regional improvements in model fit are particularly striking for sea level histories along the west coast of North America in the region of the former CIS. We suggest that here, it is possible that the observed rapid fall in sea level following deglaciation is not solely due to the low mantle viscosities expected for the Cascadia subduction zone, but also due to a component of transient mantle relaxation. Improvements in fit to the RSL data in Profile 1 are also achieved when transient deformation is included in Earth models with a reduced upper mantle viscosity (Figures S12–S13 in Supporting Information S1), suggesting that in the Cascadia subduction zone both reduced viscosity and transient deformation may be present.

Sites like Richmond Gulf and Ångermanland are located at or near the center of past ice sheets and are also sensitive to inclusion of transient mantle relaxation. Although variations in lithospheric thickness should also be considered, the Burgers models used in this study appear to have at least some ability to better predict sea level fall at these locations. In farther field locations, the model predictions are much less sensitive to the inclusion of transient deformation, which limits the ability of even well-constrained sea level records to distinguish between model cases. Interestingly, a recent study by Kang et al. (2020) showed that similar sensitivities in RSL records were predicted by models that included a 3D nonlinear description of mantle viscosity. Ultimately, the underlying inference of both this study and that of Kang et al. (2020) is that a Maxwell model misses a component of timescale dependent deformation in the mantle that may be identifiable in certain well-constrained records of sea level change.

We also compare the effect of varying which layers in the mantle include transient deformation (whole mantle vs. only upper mantle or lower mantle). When improvements in model fit to data are obtained, much of the improvement comes from the transient deformation in the lower mantle; a smaller but nonnegligible improvement in fit is obtained when the transient deformation is restricted to the upper mantle (Figures 6 and 7). The result is that the models with transient deformation included in the whole mantle yield the best fits at most of the selected RSL locations. However, at some sites, there is little difference between the WM and LM model variations.

This study has provided a first overview of Earth model parameter space to evaluate whether transient rheology deserves more attention in GIA modeling studies. As such, there are refinements to the approach that future work can address. More complex Earth model variations could examine the interplay between transient deformation and the addition of low viscosity mantle layers expected in subduction zones (Hu & Freymueller, 2019; James, Gowan, Wada, & Wang, 2009). Alternatively, the inclusion of additional Kelvin elements in an extended Burgers body (Ivins et al., 2020; Lau & Holtzman, 2019) may provide a description of Earth rheology more consistent with rock physics experiments (Faul & Jackson, 2015), as well as allow for deformation over a range of forcing frequencies. Although, as with the simple Burgers body, parameter constraint in an EBM may be difficult. As we have used only the ICE-7G ice model, the effect of variations in ice model also could be examined. For example, regional improvements of the deglaciation timing history of the CIS may further reconcile misfits of model predictions with data in this region (James et al., 2000). As well, misfits between models and data at Arisaig (Figures 4 and 5) suggest possible deficiencies in the ice sheet model here. Indeed, several studies have focused on improving regional ice sheet models of the BIIS (Bradley et al., 2011; Kuchar et al., 2012); adoption of a regionally developed ice sheet history may improve the fit of models to data in this region. Finally, many of our preliminary conclusions are made possible by the collection of new RSL data, like that along Profile 1, as well as the reevaluation and open publication of older data (Khan et al., 2019). Future collection of additional sea level indicators will help to extend or revise the results presented here.

We recognize that achieving a better fit of model predictions to RSL data is not incontrovertible evidence that transient deformation in the mantle is an important process to include in GIA models. This is because the coupling between ice model and Earth model combinations leaves considerable uncertainty in the GIA problem, such that variations to one component can affect best-fit inferences for the other component. However, the results suggest

that good quality RSL data are sensitive enough to distinguish in some settings between strictly steady-state deformation and deformation that also includes a transient component of mantle relaxation.

6. Conclusions

We study the temporal behavior of transient deformation arising from Burgers models and compare to several RSL histories. Compared to Maxwell models, Burgers models predict a short-lived phase of fast deformation after a load change. Here, the relative magnitude of the Kelvin rigidity compared to the elastic Maxwell rigidity plays a major role in the amount of transient deformation and thus RSL change. Comparing Burgers and Maxwell model results to high quality RSL data, we find that the transient deformation that results from Burgers models better explains the rapid sea level drop that is observed after deglaciation in sites underneath or adjacent to former ice sheets. Therefore, transient deformation should at least be considered as another possible process of interest in GIA models that seek to constrain GIA signals, particularly in near-field locations.

Data Availability Statement

All of the relative sea level data used in this work are already available and published within the references provided in the caption to Figure 2 for sites 1–14 (1 = James et al., 2005, 2 = Hutchinson et al., 2004, 3 = James, Gowan, Hutchinson, et al., 2009, 4 = Engelhart et al., 2015, 5 = Vacchi et al., 2018, 6–7 = Engelhart and Horton, 2012, 8 = Milliken et al., 2008, 9 = Nordman et al., 2015, 10–11 = Shennan et al., 2018, 12 = Hijma and Cohen, 2019, 13 = Peltier and Fairbanks, 2006, and 14 = Mann et al., 2019).

Acknowledgments
We thank Erik Ivins and an anonymous reviewer for comments which substantially improved the manuscript. This work is funded by the Netherlands Organization for Scientific Research GO Programma Grant ALWGO.2017.005 and by the TU Delft SESeaL project (Karen Simon) and ALWGO.2018.038 (Taco Broerse).

References

Adhikari, S., Milne, G. A., Caron, L., Khan, S. A., Kjeldsen, K. K., Nilsson, J., et al. (2021). Decadal to centennial timescale mantle viscosity inferred from modern crustal uplift rates in Greenland. *Geophysical Research Letters*, *48*(19), e2021GL094040. https://doi.org/10.1029/2021gl094040

Bradley, S. L., Milne, G. A., Shennan, I., & Edwards, R. (2011). An improved glacial isostatic adjustment model for the British Isles. *Journal of Quaternary Science*, *26*(5), 541–552. https://doi.org/10.1002/jqs.1481

Broerse, T., Riva, R., Simons, W., Govers, R., & Vermeersen, B. (2015). Postseismic GRACE and GPS observations indicate a rheology contrast above and below the Sumatra slab. *Journal of Geophysical Research: Solid Earth*, *120*(7), 5343–5361. https://doi.org/10.1002/2015jb011951

Burgers, J. M. (1935). *Mechanical considerations, model systems, phenomenological theories of relaxation and viscosity*. First Report on Viscosity and Plasticity (pp. 21–33). Akademie van Wetenschappen.

Caron, L., Métivier, L., Greff-Lefftz, M., Fleitout, L., & Rouby, H. (2017). Inverting Glacial Isostatic Adjustment signal using Bayesian framework and two linearly relaxing rheologies. *Geophysical Journal International*, *209*(2), 1126–1147. https://doi.org/10.1093/gji/ggx083

Chopra, P. N. (1997). High-temperature transient creep in olivine rocks. *Tectonophysics*, *279*(1–4), 93–111. https://doi.org/10.1016/s0040-1951(97)00134-0

D'Agostino, G., Spada, G., & Sabadini, R. (1997). Postglacial rebound and lateral viscosity variations: A semi-analytical approach based on a spherical model with Maxwell rheology. *Geophysical Journal International*, *129*(3), F9–F13. https://doi.org/10.1111/j.1365-246x.1997.tb04487.x

Dziewonski, A. M., & Anderson, D. L. (1981). Preliminary reference Earth model. *Physics of the Earth and Planetary Interiors*, *25*(4), 297–356. https://doi.org/10.1016/0031-9201(81)90046-7

Engelhart, S. E., & Horton, B. P. (2012). Holocene sea level database for the Atlantic coast of the United States. *Quaternary Science Reviews*, *54*, 12–25. https://doi.org/10.1016/j.quascirev.2011.09.013

Engelhart, S. E., Vacchi, M., Horton, B. P., Nelson, A. R., & Kopp, R. E. (2015). A sea-level database for the Pacific coast of central North America. *Quaternary Science Reviews*, *113*, 78–92. https://doi.org/10.1016/j.quascirev.2014.12.001

Faul, U., & Jackson, I. (2015). Transient creep and strain energy dissipation: An experimental perspective. *Annual Review of Earth and Planetary Sciences*, *43*(1), 541–569. https://doi.org/10.1146/annurev-earth-060313-054732

Freed, A. M., Hirth, G., & Behn, M. D. (2012). Using short-term postseismic displacements to infer the ambient deformation conditions of the upper mantle. *Journal of Geophysical Research*, *117*(B1), B01409. https://doi.org/10.1029/2011jb008562

Han, S.-C., Sauber, J., Luthcke, S. B., Ji, C., & Pollitz, F. F. (2008). Implications of postseismic gravity change following the great 2004 Sumatra-Andaman earthquake from the regional harmonic analysis of GRACE intersatellite tracking data. *Journal of Geophysical Research*, *113*(B11), B11413. https://doi.org/10.1029/2008jb005705

Hansen, L. N., Wallis, D., Breithaupt, T., Thom, C. A., & Kempton, I. (2021). Dislocation creep of olivine: Backstress evolution controls transient creep at high temperatures. *Journal of Geophysical Research: Solid Earth*, *126*(5), e2020JB021325. https://doi.org/10.1029/2020jb021325

Hanson, D. R., & Spetzler, H. A. (1994). Transient creep in natural and synthetic, iron-bearing olivine single crystals: Mechanical results and dislocation microstructures. *Tectonophysics*, *235*(4), 293–315. https://doi.org/10.1016/0040-1951(94)90191-0

Hetland, E. A., & Hager, B. H. (2006). The effects of rheological layering on post-seismic deformation. *Geophysical Journal International*, *166*(1), 277–292. https://doi.org/10.1111/j.1365-246X.2006.02974.x

Hijma, M. P., & Cohen, K. M. (2019). Holocene sea-level database for the Rhine-Meuse Delta, The Netherlands: Implications for the pre-8.2 ka sea-level jump. *Quaternary Science Reviews*, *214*, 68–86. https://doi.org/10.1016/j.quascirev.2019.05.001

Hijma, M. P., Horton, B. P., Engelhart, S. E., Törnqvist, T. E., Hu, P., & Hill, D. F. (2015). A protocol for a geological sea-level database. In I. Shennan, A. J. Long, & B. P. Horton (Eds.), *Handbook of sea-level research* (pp. 536–553). John Wiley & Sons, Ltd.

Hoechner, A., Sobolev, S. V., Einarsson, I., & Wang, R. (2011). Investigation on afterslip and steady state and transient rheology based on post-seismic deformation and geoid change caused by the Sumatra 2004 earthquake. *Geochemistry, Geophysics, Geosystems*, *12*(7). https://doi.org/10.1029/2010gc003450

Hu, Y., & Freymueller, J. T. (2019). Geodetic observations of time-variable glacial isostatic adjustment in southeast Alaska and its implications for Earth rheology. *Journal of Geophysical Research: Solid Earth*, *124*(9), 9870–9889. https://doi.org/10.1029/2018jb017028

Hutchinson, I., James, T., Clague, J., Barrie, J. V., & Conway, K. (2004). Reconstruction of late Quaternary sea-level change in southwestern British Columbia from sediments in isolation basins. *Boreas*, *33*(3), 183–194. https://doi.org/10.1080/03009480410001299

Ivins, E. R., Caron, L., Adhikari, S., & Larour, E. (2022). Notes on a compressible extended Burgers model of rheology. *Geophysical Journal International*, *228*(3), 1975–1991. https://doi.org/10.1093/gji/ggab452

Ivins, E. R., Caron, L., Adhikari, S., Larour, E., & Scheinert, M. (2020). A linear viscoelasticity for decadal to centennial time scale mantle deformation. *Reports on Progress in Physics*, *83*(10), 106801. https://doi.org/10.1088/1361-6633/aba346

James, T., Gowan, E. J., Hutchinson, I., Clague, J. J., Barrie, J. V., & Conway, K. W. (2009). Sea-level change and paleogeographic reconstructions, southern Vancouver Island, British Columbia, Canada. *Quaternary Science Reviews*, *28*(13–14), 1200–1216. https://doi.org/10.1016/j.quascirev.2008.12.022

James, T. S. (1991). *Post-glacial deformation. PhD thesis*. Princeton University.

James, T. S., Clague, J. J., Wang, K., & Hutchinson, I. (2000). Postglacial rebound at the northern Cascadia subduction zone. *Quaternary Science Reviews*, *19*(14–15), 1527–1541. https://doi.org/10.1016/s0277-3791(00)00076-7

James, T. S., Gowan, E. J., Wada, I., & Wang, K. (2009). Viscosity of the asthenosphere from glacial isostatic adjustment and subduction dynamics at the northern Cascadia subduction zone, British Columbia, Canada. *Journal of Geophysical Research*, *114*(B4), B04405. https://doi.org/10.1029/2008jb006077

James, T. S., Hutchinson, I., Vaughn Barrie, J., Conway, K. W., & Mathews, D. (2005). Relative sea-level change in the northern Strait of Georgia, British Columbia. *Géographie Physique et Quaternaire*, *59*(2–3), 113–127. https://doi.org/10.7202/014750ar

Kang, K., Zhong, S., & Geruo, A. (2020). *The effects of non-Newtonian rheology in the upper mantle on GIA observables*. American Geophysical Union Fall Meeting.

Karato, S. (1998). Micro-physics of post glacial rebound. In P. Wu (Ed.), *Dynamics of the Ice Age Earth: A modern perspective* (pp. 351–364). Trans Tech Publications.

Karato, S. I. (2021). A theory of inter-granular transient dislocation creep: Implications for the geophysical studies on mantle rheology. *Journal of Geophysical Research: Solid Earth*, *126*(10). https://doi.org/10.1029/2021jb022763

Karato, S.-I., & Wu, P. (1993). Rheology of the upper mantle: A synthesis. *Science*, *260*(5109), 771–778. https://doi.org/10.1126/science.260.5109.771

Khan, N. S., Horton, B. P., Engelhart, S., Rovere, A., Vacchi, M., Ashe, E. L., et al. (2019). Inception of a global atlas of sea levels since the Last Glacial Maximum. *Quaternary Science Reviews*, *220*, 359–371. https://doi.org/10.1016/j.quascirev.2019.07.016

Kuchar, J., Milne, G., Hubbard, A., Patton, H., Bradley, S., Shennan, I., & Edwards, R. (2012). Evaluation of a numerical model of the British-Irish ice sheet using relative sea-level data: Implications for the interpretation of trimline observations. *Journal of Quaternary Science*, *27*(6), 597–605. https://doi.org/10.1002/jqs.2552

Lambeck, K., Smither, C., & Johnston, P. (1998). Sea-level change, glacial rebound and mantle viscosity for northern Europe. *Geophysical Journal International*, *134*(1), 102–144. https://doi.org/10.1046/j.1365-246x.1998.00541.x

Lau, H. C. P., & Holtzman, B. K. (2019). "Measures of dissipation in viscoelastic media" extended: Toward continuous characterization across very broad geophysical time scales. *Geophysical Research Letters*, *46*(16), 9544–9553. https://doi.org/10.1029/2019gl083529

Lau, H. C. P., Holtzman, B. K., & Havlin, C. (2020). Toward a self-consistent characterization of lithospheric plates using full-spectrum viscoelasticity. *AGU Advances*, *1*(4), e2020AV000205. https://doi.org/10.1029/2020AV000205

Mann, T., Bender, M., Lorscheid, T., Stocchi, P., Vacchi, M., Switzer, A. D., & Rovere, A. (2019). Holocene sea levels in Southeast Asia, Maldives, India and Sri Lanka: The SEAMIS database. *Quaternary Science Reviews*, *219*, 112–125. https://doi.org/10.1016/j.quascirev.2019.07.007

Marsman, C. P., van der Wal, W., Riva, R. E. M., & Freymueller, J. T. (2021). The impact of a 3-D Earth structure on glacial isostatic adjustment in Southeast Alaska following the Little Ice Age. *Journal of Geophysical Research: Solid Earth*, *126*(12), e2021JB022312. https://doi.org/10.1029/2021jb022312

Martinec, Z., Klemann, V., van der Wal, W., Riva, R. E. M., Spada, G., Sun, Y., et al. (2018). A benchmark study of numerical implementations of the sea level equation in GIA modelling. *Geophysical Journal International*, *215*(1), 389–414. https://doi.org/10.1093/gji/ggy280

Milliken, K. T., Anderson, J. B., & Rodriguez, A. B. (2008). A new composite Holocene sea-level curve for the northern Gulf of Mexico. Special paper 443: Response of upper gulf coast estuaries to Holocene climate change and sea-level rise (pp. 1–11).

Morris, S. J. S., & Jackson, I. (2009). Diffusionally assisted grain-boundary sliding and viscoelasticity of polycrystals. *Journal of the Mechanics and Physics of Solids*, *57*(4), 744–761. https://doi.org/10.1016/j.jmps.2008.12.006

Muto, J., Moore, J. D. P., Barbot, S., Iinuma, T., Ohta, Y., & Iwamori, H. (2019). Coupled afterslip and transient mantle flow after the 2011 Tohoku earthquake. *Science Advances*, *5*(9). https://doi.org/10.1126/sciadv.aaw1164

Nordman, M., Milne, G., & Tarasov, L. (2015). Reappraisal of the Ångerman River decay time estimate and its application to determine uncertainty in Earth viscosity structure. *Geophysical Journal International*, *201*(2), 811–822. https://doi.org/10.1093/gji/ggv051

Paulson, A., Zhong, S., & Wahr, J. (2007). Inference of mantle viscosity from GRACE and relative sea level data. *Geophysical Journal International*, *171*(2), 497–508. https://doi.org/10.1111/j.1365-246X.2007.03556.x

Peltier, W. R. (1974). The impulse response of a Maxwell Earth. *Reviews of Geophysics and Space Physics*, *12*(4), 649–669. https://doi.org/10.1029/rg012i004p00649

Peltier, W. R. (1985). The LAGEOS constraint on deep mantle viscosity: Results from a new normal mode method for the inversion of viscoelastic relaxation spectra. *Journal of Geophysical Research*, *90*(B11), 9411–9421. https://doi.org/10.1029/jb090ib11p09411

Peltier, W. R. (2004). Global glacial isostasy and the surface of the ice-age Earth: The ICE-5G (VM2) model and GRACE. *Annual Review of Earth and Planetary Sciences*, *32*(1), 111–149. https://doi.org/10.1146/annurev.earth.32.082503.144359

Peltier, W. R., Argus, D. F., & Drummond, R. (2015). Space geodesy constrains ice age terminal deglaciation: The global ICE-6G_C (VM5a) model. *Journal of Geophysical Research: Solid Earth*, *120*(1), 450–487. https://doi.org/10.1002/2014jb011176

Peltier, W. R., Drummond, R. A., & Tushingham, A. M. (1986). Post-glacial rebound and transient lower mantle rheology. *Geophysical Journal of the Royal Astronomical Society*, *87*(1), 79–116. https://doi.org/10.1111/j.1365-246x.1986.tb04548.x

Peltier, W. R., & Fairbanks, R. G. (2006). Global glacial ice volume and Last Glacial Maximum duration from an extended Barbados sea level record. *Quaternary Science Reviews*, *25*(23–24), 3322–3337. https://doi.org/10.1016/j.quascirev.2006.04.010

Peltier, W. R., Yuen, D. A., & Wu, P. (1980). Postglacial rebound and transient rheology. *Geophysical Research Letters*, *7*(10), 733–736. https://doi.org/10.1029/gl007i010p00733

Pollitz, F. F. (2005). Transient rheology of the upper mantle beneath central Alaska inferred from the crustal velocity field following the 2002 Denali earthquake. *Journal of Geophysical Research*, *110*(B8), B08407. https://doi.org/10.1029/2005jb003672

Ranalli, G. (1987). *Rheology of the earth: Deformation and flow processes in geophysics and geodynamics* (p. 366). Allen & Unwin Inc.

Roy, K., & Peltier, W. R. (2018). Relative sea level in the Western Mediterranean basin: A regional test of the ICE-7G_NA (VM7) model and a constraint on late Holocene Antarctic deglaciation. *Quaternary Science Reviews*, *183*, 76–87. https://doi.org/10.1016/j.quascirev.2017.12.021

Rümpker, G., & Wolf, D. (1996). Viscoelastic relaxation of a Burgers half-space: Implications for the interpretation of the Fennoscandian uplift. *Geophysical Journal International*, *124*(2), 541–555. https://doi.org/10.1111/j.1365-246x.1996.tb07036.x

Sabadini, R., Vermeersen, B., & Cambiotti, G. (2016). *Global dynamics of the earth: Applications of viscoelastic relaxation theory to solid-earth and planetary geophysics* (358 pp.). Springer Science+Business Media.

Sabadini, R., Yuen, D. A., & Gasperini, P. (1985). The effects of transient rheology on the interpretation of lower mantle viscosity. *Geophysical Research Letters*, *12*(6), 361–364. https://doi.org/10.1029/gl012i006p00361

Shennan, I., Bradley, S. L., & Edwards, R. (2018). Relative sea-level changes and crustal movements in Britain and Ireland since the Last Glacial Maximum. *Quaternary Science Reviews*, *188*, 143–159. https://doi.org/10.1016/j.quascirev.2018.03.031

Smith, B. K., & Carpenter, F. O. (1987). Transient creep in orthosilicates. *Physics of the Earth and Planetary Interiors*, *49*(3–4), 314–324. https://doi.org/10.1016/0031-9201(87)90033-1

Spada, G., Antonioli, A., Cianetti, S., & Giunchi, C. (2006). Glacial isostatic adjustment and relative sea-level changes: The role of lithospheric and upper mantle heterogeneities in a 3-D spherical Earth. *Geophysical Journal International*, *165*(2), 692–702. https://doi.org/10.1111/j.1365-246X.2006.02969.x

Spada, G., Colleoni, F., & Ruggieri, G. (2011). Shallow upper mantle rheology and secular ice sheet fluctuations. *Tectonophysics*, *511*(3–4), 89–98. https://doi.org/10.1016/j.tecto.2009.12.020

Tan, B. H., Jackson, I., & Gerald, J. D. F. (2001). High-temperature viscoelasticity of fine-grained polycrystalline olivine. *Physics and Chemistry of Minerals*, *28*(9), 641–664. https://doi.org/10.1007/s002690100189

Tushingham, A. M., & Peltier, W. R. (1991). Ice-3G: A new global model of late pleistocene deglaciation based upon geophysical predictions of post-glacial relative sea level change. *Journal of Geophysical Research*, *96*(B3), 4497–4523. https://doi.org/10.1029/90jb01583

Vacchi, M., Engelhart, S. E., Nikitina, D., Ashe, E. L., Peltier, W. R., Roy, K., et al. (2018). Postglacial relative sea-level histories along the eastern Canadian coastline. *Quaternary Science Reviews*, *201*, 124–146. https://doi.org/10.1016/j.quascirev.2018.09.043

van der Wal, W., Wu, P., Wang, H., & Sideris, M. G. (2010). Sea levels and uplift rate from composite rheology in glacial isostatic adjustment modeling. *Journal of Geodynamics*, *50*(1), 38–48. https://doi.org/10.1016/j.jog.2010.01.006

Vermeersen, L. L. A., & Sabadini, R. (1997). A new class of stratified viscoelastic models by analytical techniques. *Geophysical Journal International*, *129*(3), 531–570. https://doi.org/10.1111/j.1365-246x.1997.tb04492.x

Wallis, D., Hansen, L. N., Wilkinson, A. J., & Lebensohn, R. A. (2021). Dislocation interactions in olivine control postseismic creep of the upper mantle. *Nature Communications*, *12*(1), 3496. https://doi.org/10.1038/s41467-021-23633-8

Whitehouse, P. L. (2018). Glacial isostatic adjustment modelling: Historical perspectives, recent advances, and future directions. *Earth Surface Dynamics*, *6*(2), 401–429. https://doi.org/10.5194/esurf-6-401-2018

Wu, P. (1993). Postglacial rebound in a power-law medium with axial symmetry and the existence of the transition zone in relative sea-level data. *Geophysical Journal International*, *114*(3), 417–432. https://doi.org/10.1111/j.1365-246x.1993.tb06976.x

Yuen, D. A., & Peltier, W. R. (1982). Normal modes of the viscoelastic Earth. *Geophysical Journal of the Royal Astronomical Society*, *69*(2), 495–526. https://doi.org/10.1111/j.1365-246x.1982.tb04962.x

Yuen, D. A., Sabadini, R. C. A., Gasperini, P., & Boschi, E. (1986). On transient rheology and glacial isostasy. *Journal of Geophysical Research*, *91*(B11), 11420–11438. https://doi.org/10.1029/jb091ib11p11420